

Microwave Synthesis of a Photocatalytically Active SnO-Based Material

S. A. Kuznetsova, A. A. Pichugina, and V. V. Kozik

Tomsk State University, pr. Lenina 36, Tomsk, 634050 Russia

e-mail: alina.com@mail.ru

Received September 19, 2013

Abstract—Tin(II) oxide nanopowder has been prepared through microwave processing of an ammoniacal $\text{Sn}_6\text{O}_4(\text{OH})_4$ suspension, and the effect of synthesis duration on the surface morphology, acid–base properties, and photocatalytic activity of the SnO has been examined. The results demonstrate that the surface morphology plays a key role in determining the photocatalytic activity of powder SnO for methyl orange photodegradation.

DOI: 10.1134/S0020168514040086

INTRODUCTION

Microwave processing is a promising method widely used to prepare oxide materials [1–4]. In contrast to conventional heat-treatment processes, microwave processing considerably reduces the time needed for the dehydration and decomposition of materials and, when conducted in air, may lead to the formation of oxides with unstable oxidation states [5]. A number of studies [4–6] were concerned with the preparation of tin(II) oxide through the decomposition of tin(II) hydroxy compounds by microwave processing in air. The lack of SnO oxidation to SnO_2 was attributed by Dien-She Wu et al. [6] to the different microwave absorption intensities in the oxides (SnO has stronger microwave absorption). Available experimental data on SnO preparation are insufficient for assessing the effect of microwave radiation on the surface morphology and properties of SnO.

Among the many properties of semiconducting oxides, particular attention has recently been paid to their photocatalytic activity, which contributes to the decomposition of organic contaminants in waste water [7, 8], where methyl orange photodegradation in aqueous oxide suspensions is used mainly as a model system.

In connection with this, the purpose of this work was to study the effect of microwave synthesis time on the surface morphology and photocatalytic activity of SnO.

EXPERIMENTAL

The starting suspension (precursor) was prepared by dissolving metallic tin in concentrated hydrochloric acid, followed by Sn^{2+} precipitation with 25% aqueous ammonia at pH 10–12. Next, four series of samples of the suspension were subjected to microwave process-

ing in a 539-W oven (2450 MHz) for 3, 5, 7, and 15 min (series 1, 2, 3, and 4, respectively). The samples were then washed with distilled water, centrifuged, and dried at 90°C.

The solid phase in the suspension and the final synthesis products (oxides) were characterized by X-ray diffraction (XRD) on a Rigaku Miniflex 600 diffractometer (CuK_α radiation, $2\theta = 10^\circ\text{--}90^\circ$, scan step of 0.02° , scan rate of 5 deg/min). JCPDS PDF data were used to index diffraction peaks, evaluate the crystallite size, and determine the quantitative phase composition of the samples. The specific surface area of the synthesized tin(II) oxide powders was determined by BET analysis of low-temperature nitrogen sorption isotherms obtained using a TriStar II automatic gas adsorption analyzer (relative uncertainty $\Delta \pm 10\%$). Surface morphologies were examined by scanning electron microscopy on a Hitachi TM-3000 operated at an accelerating voltage of 15 kV with surface charge elimination (electron gun: 5×10^2 Pa; sample chamber: 30–50 Pa), using a QUANTAX 70 energy dispersive spectrometer system. The uncertainty in quantitative elemental analysis was $\pm 5\%$. The acid–base properties of the synthesized oxides were studied using a Multitest pH meter by a procedure described elsewhere [9].

The photocatalytic activity of the SnO powders was assessed for methyl orange azo dye photodegradation. The SnO powders were mixed with an aqueous solution of the dye. To reach sorption–desorption equilibrium, the mixture was stirred in the dark, then placed under an I_2 excimer ultraviolet lamp (I_2BD_P Model) with $\lambda_{\text{max}} = 342$ nm, and exposed to ultraviolet (UV) radiation for 60 min with constant stirring. The absorbance of the samples was measured at 10-min intervals (0, 10, 20, 30, 40, 50, and 60 min). After the beginning of an experiment, we took aliquots, which

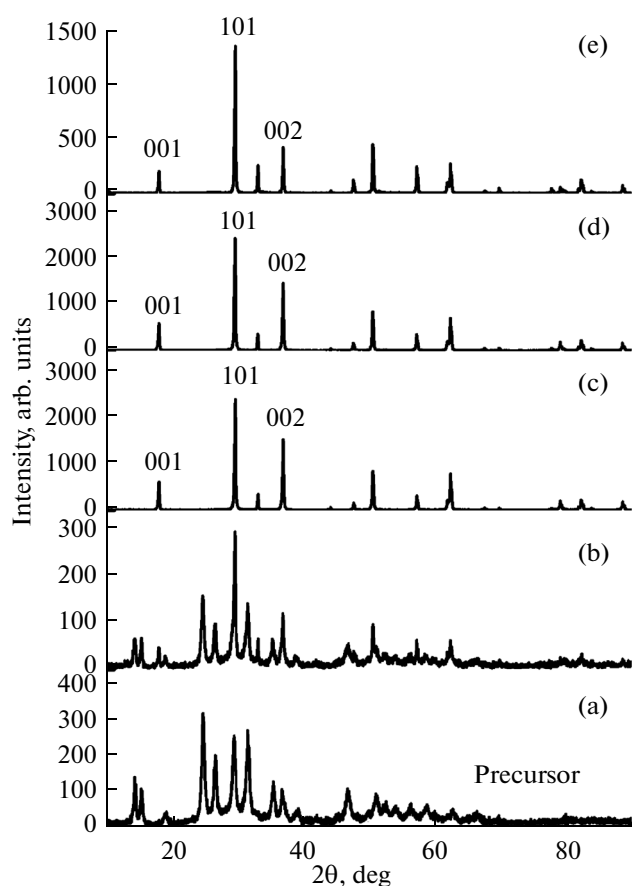


Fig. 1. XRD patterns of (a) the precursor and samples (b) 1, (c) 2, (d) 3, and (e) 4.

were centrifuged to separate the precipitate. From the variation in absorbance, we assessed the extent of methyl orange decomposition. The methyl orange concentration was determined spectrophotometrically on a PE-5400UF spectrophotometer using the QA5400 quantitative analysis program and was evaluated from the height of the absorption peak at $\lambda = 461$ nm.

The composition of the methyl orange decomposition products after UV exposure was determined using a Surveyor high-performance liquid chromatography (HPLC) system equipped with an autosampler and an LCQ Advantage MAX mass spectrometric detector. Components were separated in a HyperSil Gold column packed with a reversed phase sorbent (C18) grafted on silica gel with a particle size of 5 μm . The eluents used were aqueous formic acid (0.1 wt %) and acetonitrile (100 wt %). The eluent flow rate was 0.5 mL/min.

RESULTS AND DISCUSSION

According to XRD data (Fig. 1a), the precursor had the form of an ammoniacal solution based on

$\text{Sn}_6\text{O}_4(\text{OH})_4$ powder (PDF no. 01-084-2157) with a tetragonal structure and lattice parameters $a = b = 7.962151$ nm and $c = 9.142758$ nm. Microwave processing of the solution for 3 min in a 539-W oven led to the onset of $\text{Sn}_6\text{O}_4(\text{OH})_4$ decomposition and the formation of a mixture of 17 wt % tetragonal SnO (PDF no. 01-072-101, $a = b = 0.3809703$ nm, $c = 0.4849768$ nm) and 83 wt % $\text{Sn}_6\text{O}_4(\text{OH})_4$ ($a = b = 8.005666$ nm, $c = 9.152423$ nm) (Fig. 1b). Increasing the microwave processing time of the ammoniacal $\text{Sn}_6\text{O}_4(\text{OH})_4$ solution led to the formation of a single-phase product, which was identified by XRD (Fig. 1c) as SnO, with a crystallite size of 46 nm in the (101) plane and 40 nm along (002). It can be seen from Figs. 1d and 1e that increasing the microwave processing time of the starting suspension had no effect on the composition of the final product but increased the crystallite size to 49 nm in both growth directions of SnO. Moreover, it can be seen from the XRD patterns in Fig. 1 that the intensity of the peaks corresponding to the growth of the SnO crystal along the z axis (in an hkl plane (001, 002)) decreases with an increase in the microwave processing time of the suspension. Therefore, after nucleation accompanying the $\text{Sn}_6\text{O}_4(\text{OH})_4$ decomposition, the SnO crystallites grew predominantly in the direction of the hkl plane (001, 002), whereas increasing the processing time led to the growth of the crystallites in the direction of the hkl plane (101). In this process, the anisotropy coefficient, calculated as the ratio of the crystallite size in the (002) plane to that along (101), varied from 0.86 to 1.

As seen in Fig. 2, the microwave processing time of the precursor had little effect on the surface morphology of the SnO samples. Qualitative and quantitative surface morphology analysis data are supported by XRD results. Microwave processing for 3 min led to partial formation of tin(II) oxide agglomerates (Fig. 2a), which had the form of tetragonal plates. Single-phase SnO was formed after microwave processing of the precursor for 5 min. According to quantitative analysis data, the Sn : O ratio at each point of samples 2 was about 1 : 1 (51.65 at % Sn and 48.34 at % O). All of the SnO samples obtained (series 2–4) had the form of tetragonal plates with a layered structure, ranging in size from 100 to 200 nm. Their specific surface area and average pore size were 3.0 m^2/g and 18 nm, respectively.

Even though the samples were identical in specific surface area and crystallite geometry, they differed in acid–base properties. The pH_{eq} of the aqueous suspension was 3.86 for samples 4, 5.80 for samples 3, and 6.1 for samples 2. These results indicate that all of the SnO samples were solid Lewis acids but differed in the surface density of Lewis acid centers [9]. This can be accounted for in terms of different surface defect densities [9], for example, because of the formation of different types of pores in the tin(II) oxide, as evidenced

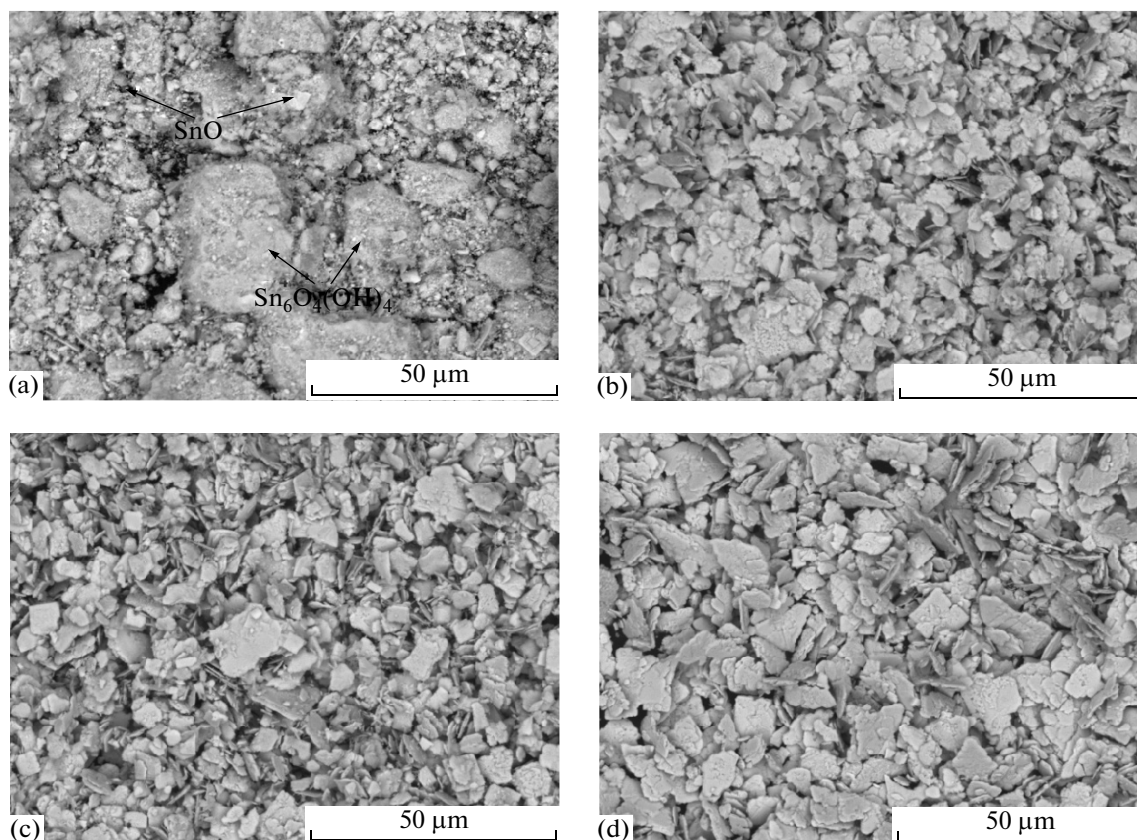


Fig. 2. Micrographs of samples (a) 1, (b) 2, (c) 3, and (d) 4.

by the shape of the nitrogen adsorption–desorption isotherms of our samples (Fig. 3). According to data in the literature [10, 11], the shape of the sorption–desorption hysteresis loop for samples 4 (Fig. 3b) corresponds to a mesoporous adsorbent nonuniform in pore size and shape. The shape of the hysteresis loop for samples 2 suggests the presence of slit pores in the SnO powder.

The present results on the photocatalytic activity of SnO for methyl orange decomposition demonstrate that, among the samples studied, the highest photocatalytic activity was exhibited by samples 4. In particular, after holding these samples in an azo dye solution, the tin(II) oxide surface sorbed up to 50 wt % of the methyl orange. According to spectrophotometry data, subsequent UV exposure led to methyl orange decomposition. After 60 min of exposure in the presence of samples 4, the degree of methyl orange decomposition was as high as 95%. In the presence of samples 2 and 3, the degree of azo dye decomposition in 60 min was 45 and 73%, respectively (Fig. 4). A comparative analysis of HPLC/MS spectra of the methyl orange before photocatalysis (Fig. 5) and mass

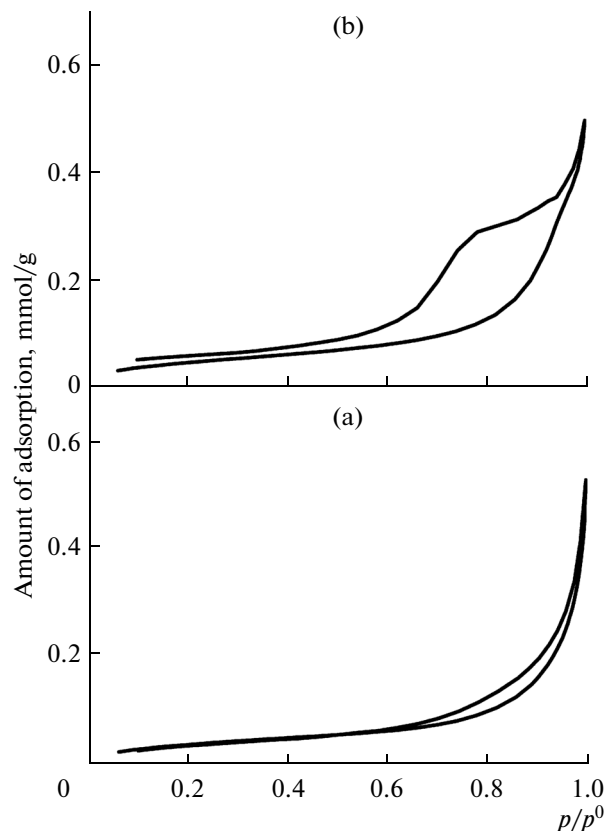


Fig. 3. Adsorption–desorption isotherms of samples (a) 2 and (b) 4.

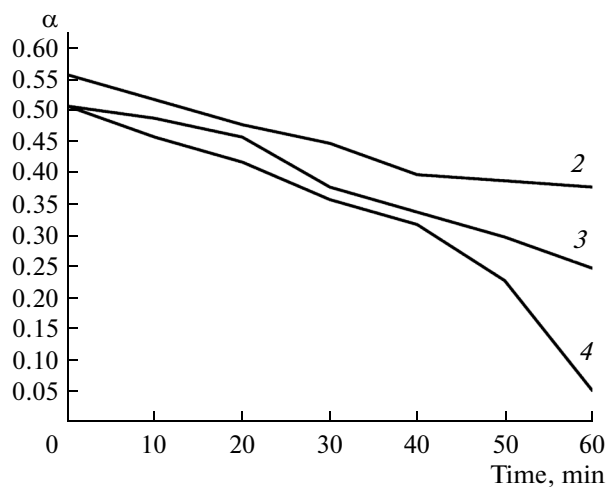


Fig. 4. Degree of conversion as a function of time for the photocatalytic decomposition of methyl orange in the presence of samples 2–4.

spectra of the positively charged species formed after the photocatalysis (Fig. 6) showed that, after 50 min, the major methyl orange decomposition products were positively charged species with molecular weights from 224 to 154. The structures of some of them are presented in Fig. 6.

Our findings indicate that, all other factors being the same, the duration of the microwave synthesis of tin(II) oxide from an ammoniacal $\text{Sn}_6\text{O}_4(\text{OH})_4$ sus-

pension influences its acid–base properties and photocatalytic activity.

CONCLUSIONS

The present results demonstrate that the duration of the microwave synthesis of SnO determines its surface morphology through an increase in anisotropy coefficient. At a given specific surface area and pore size, the main factor influencing the photocatalytic

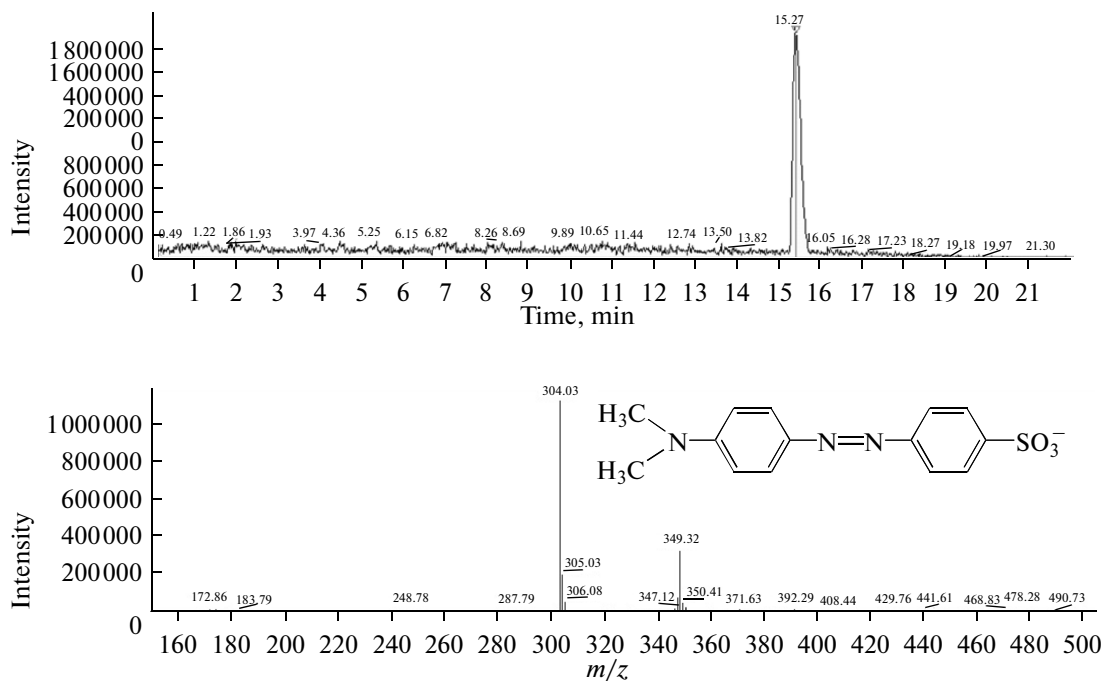


Fig. 5. HPLC/MS data for methyl orange.

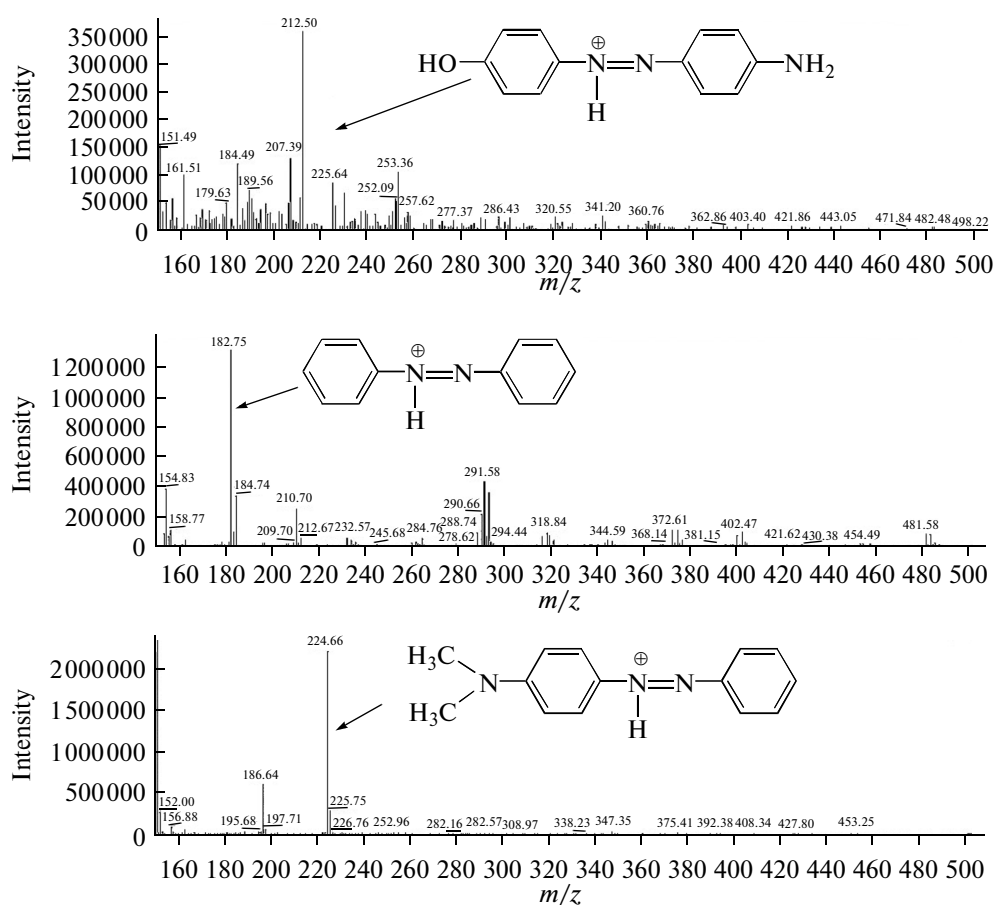


Fig. 6. Mass spectra of positively charged species after UV-induced methyl orange decomposition.

activity of SnO is the pore shape. It is worth noting that the acid properties of the surface of powder SnO are related to its photocatalytic activity for methyl orange azo dye photodegradation.

REFERENCES

1. Karimov, O.Kh., Daminev, R.R., Kas'yanova, L.Z., et al., Application of microwave radiation in the fabrication of metal oxide catalysts, *Fundam. Issled.*, 2013, no. 4, p. 801.
2. Balakhonov, S.V., Ivanov, V.K., Baranchikov, A.E., et al., A comparative analysis of the physicochemical properties of vanadium-oxide-based nanomaterials prepared by hydrothermal and microwave-assisted hydrothermal processes, *Nanosist.: Fiz., Khim., Mat.*, 2012, vol. 3, no. 4, p. 66.
3. Vanetsev, A.S., Ketsko, V.A., and Tret'yakov, Yu.D., Microwave-induced microstructural evolution of individual metal oxides, *Kondens. Sredy Mezhfaznye Granitsy*, 2009, vol. 11, no. 4, p. 280.
4. Pires, F.I., Joanni, E., Savu, R., et al., Microwave-assisted hydrothermal synthesis of nanocrystalline SnO powders, *Mater. Lett.*, 2008, vol. 62, p. 239.
5. Krishnakumar, T., Pinna, N., Prasanna Kumari, K., et al., Microwave-assisted synthesis and characterization of tin oxide nanoparticles, *Mater. Lett.*, 2008, vol. 62, p. 3437.
6. Dien-She Wu, Chin-Yu Han, Shi-Yu Wang, et al., Microwave-assisted solution synthesis of SnO nanocrystallites, *Mater. Lett.*, 2002, vol. 53, p. 155.
7. Shaporev, A.S., Ivanov, V.K., Lebedev, V.A., et al., Photocatalytic activity of nanodispersed zinc oxide synthesized by hydrothermal microwave route, *Dokl. Chem.*, 2010, vol. 434, no. 1, p. 223.
8. Yuanhua He, Franz Grieser, and Muthupandian Ashokkumar, The mechanism of sonophotocatalytic degradation of methyl orange and its products in aqueous solution, *Ultrason. Sonochem.*, 2011, vol. 18, p. 974.
9. Minakova, T.S., *Adsorbtsionnye protsessy na poverkhnosti tverdykh tel* (Adsorption Processes on the Surface of Solids), Tomsk: Tomsk. Univ., 2007.
10. Gregg, S.J. and Sing, K.S.W., *Adsorption, Surface Area, and Porosity*, New York: Academic, 1982.
11. Krylov, O.V., *Geterogennyi kataliz* (Heterogeneous Catalysis), Moscow: Akademkniga, 2004, pp. 40–45.

Translated by O. Tsarev